JACS
JOURNAL OF THE AMERICAN CHEMICAL SOCIETY
pubs.acs.org/JACS
Article

Spectroscopically Visualizing the Evolution of Hydrogen-Bonding Interactions

Xianfeng Yi, Wei Chen, Yao Xiao, Fengqing Liu, Xin Yu, and Anmin Zheng*

Cite This: J. Am. Chem. Soc. 2023, 145, 27471−27479
Read Online

ABSTRACT: Understanding chemical bond variations is the soul of chemistry as it is essential for any chemical process. The evolution of hydrogen bonds is one of the most fundamental and emblematic events during proton transfer; however, its experimental visualization remains a formidable challenge because of the transient timescales. Herein, by subtly regulating the proton-donating ability of distinct proton donors (zeolites or tungstophosphoric acid), a series of different hydrogen-bonding configurations were precisely manipulated. Then, an advanced two-dimensional (2D) heteronuclear correlation nuclear magnetic resonance (NMR) spectroscopic technique was utilized to simultaneously monitor the electronic properties of proton donors and acceptors (2-^{13}C-acetone or trimethylphosphine oxide) through chemical shifts. Parabolic ^{1}H−^{13}C NMR relationships combined with single-well and double-well potential energy surfaces derived from theoretical simulations quantitatively identified the hydrogen bond types and allowed the evolution of hydrogen bonds to be visualized in diverse acid−base interaction complexes during proton transfer. Our findings provide a new perspective to reveal the nature and evolution of hydrogen bonds and confirm the superiority of 2D NMR techniques in identifying the subtle distinctions of various hydrogen-bonding configurations.

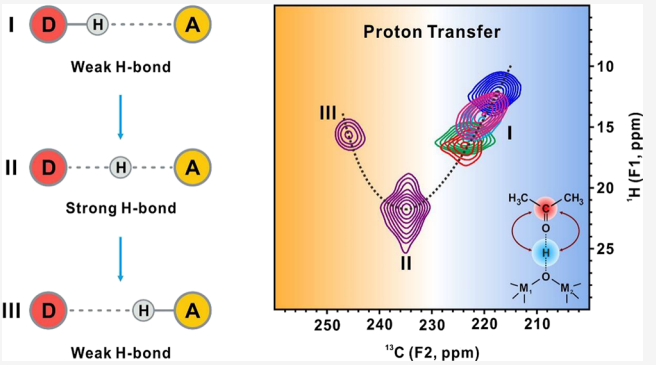

INTRODUCTION

As a magical and unique interaction in nature, the ubiquitous hydrogen bond (H-bond) is of great importance and is extensively involved in various chemical, biochemical, and material systems.[1−9] For example, the complex H-bond network in water governs its miraculous physicochemical properties.[1−3] The double helical structures of DNA are closely related to H-bonds.[4] Furthermore, the adsorption, activation, and conversion of various reactant molecules and the sequential formation of diverse intermediates and products during many important Brønsted acid-catalyzed reactions are accompanied by the dynamic variation of H-bonds as well.[6−9] Numerous experimental and theoretical techniques have been devoted to the investigation of the origins, definitions, and types of H-bonds;[10−14] however, obtaining a precise molecular description of the detailed characteristics of H-bonds is still a rather challenging task. Recently, Tokmakoff et al. carried out highly groundbreaking experiments to distinguish H-bonds and covalent bonds.[15] By using femtosecond two-dimensional (2D) infrared spectroscopy in combination with high-level quantum calculations, they demonstrated a distinct crossover in the spectroscopic signatures from conventional to strong H-bonds in aqueous FHF^-. These results touch on the foundations of chemistry and challenge our current understanding of what a chemical bond exactly is.[16] These findings also have direct implications for proton transfer processes and strongly inspire us to carry out relevant research.

Typically, an H-bond is an attractive electrostatic interaction between a proton acceptor (A) and a hydrogen atom covalently bonded to a donor (D). When the proton-donating ability of the donor is low, a weak H-bond will be formed (Scheme 1A). Upon an increase in the proton-donating ability of the donor, an increasingly stronger H-bonding interaction (intermediate H-bond; Scheme 1B) is expected, and the hydrogen atom becomes increasingly delocalized between its covalent partner and the H-bond acceptor. When the proton-donating ability of the donor is exactly comparable to that of the acceptor, the proton is precisely centered and equally shared between the donor and acceptor. This results in the formation of a strong H-bonding interaction (Scheme 1C), accompanied by the emergence of a highly delocalized proton. Upon further increasing the proton-donating ability of the donor, the proton will gradually transfer to couple with the

Received: August 10, 2023
Revised: November 7, 2023
Accepted: November 8, 2023
Published: November 22, 2023

https://doi.org/10.1021/jacs.3c08723
J. Am. Chem. Soc. 2023, 145, 27471−27479

Scheme 1. Evolution of H-Bonding Interactions during a Typical Proton Transfer Process: (A,E) a Weak H-Bond, (B,D) an Intermediate H-Bond, and (C) a Strong H-Bond.

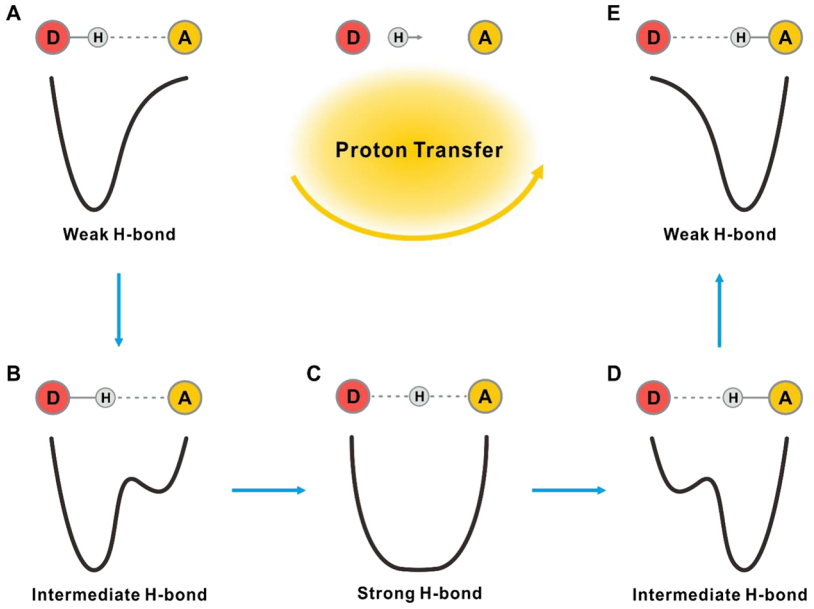

acceptor (Scheme 1D,E). Thus, the proton transfer process is achieved along with the dynamic variation of various H-bonding interactions. This is a textbook property of proton transfer. Nevertheless, to date, rare experimental evidence has been collected to clearly describe the evolution of these H-bonds because of their transient timescales during this fundamental chemical process.[17]

In response to this key issue, the primary challenge is the accurate regulation and long-term retention of various different H-bonding configurations during the proton transfer process, as illustrated in Scheme 1. Fortunately, a series of typical acidic materials (e.g., zeolites or heteropolyacids)[9,18] could be undoubtedly regarded as proton donors, whereas basic adsorbate molecules (e.g., acetone[19,20] or trimethylphosphine oxide (TMPO)[21−23]) can be certainly considered to be proton acceptors. In particular, the difference in the proton-donating abilities of various acidic materials renders the formation of diverse H-bonding configurations with subtle distinctions. This kind of ingenious host−guest interaction further plays a crucial role in maintaining their long-term stability, thus providing a feasible opportunity to precisely identify the types of H-bonding interactions and visualize their evolution by employing various analytical and spectroscopic techniques.

RESULTS AND DISCUSSION

Chemical States of Proton Donors and Acceptors in Hydrogen-Bonding Interactions. Nuclear magnetic resonance (NMR) spectroscopy has emerged as a useful and reliable tool for probing the detailed structures of various complexes. The chemical shift is an important NMR parameter reflecting the electronic properties of a specific atom in a compound, and the variation of the chemical shift is directly related to the chemical state of the involved atom.[24−33] Among these methods, ^{1}H magic angle spinning (MAS) NMR is a direct approach to identify the subtle chemical environments of hydrogen atoms in various hydrogen-containing species.[24−29] Therefore, it is anticipated that ^{1}H MAS NMR results can provide important information about the various types of H-bonding interactions between basic proton acceptors (e.g., acetone and TMPO in this work) and diverse proton donors (e.g., Brønsted acidic materials with different proton-donating abilities). The structural properties of these materials with typical acidic protons used in this study are shown in Figures S1−S3 in the Supporting Information. Among them, the ^{1}H MAS NMR spectra of dehydrated samples clearly showed the ^{1}H signals at around 4.0 ppm for zeolites and at 9.1 ppm for tungstophosphoric acid ($H_3PW_{12}O_{40}$, abbreviated as HPW), which can be undoubtedly ascribed to acidic protons[24,25] (Figure S3).

Notably, the coupling of 2-^{13}C-acetone with these protons in H-SAPO-34, H-SSZ-13, H-MOR, H-ZSM-5, and H-Beta zeolites gave rise to broad ^{1}H resonance at *ca.* 12.4, 14.0, 14.6, 16.2, and 16.7 ppm, respectively, whereas two relevant ^{1}H signals at *ca.* 15.9 and 21.8 ppm were visible when 2-^{13}C-acetone interacted with strongly acidic HPW (Figure 1A). It should be noted that the ^{1}H NMR signal at 21.8 ppm corresponds to a highly delocalized hydrogen nucleus due to the ultrastrong deshielding effect in the strong H-bonding interaction configuration. To the best of our knowledge, this may be the largest ^{1}H NMR chemical shift reported to date. Nevertheless, although all these resonances with a larger ^{1}H NMR chemical shift can be undoubtedly ascribed to the H-bonding interactions between adsorbed 2-^{13}C-acetone and acidic protons, the relationship between the observed ^{1}H NMR signal and the H-bonding type and the precise location of hydrogen atoms in various H-bonding configurations remain to be established. For example, it is unclear how to identify the 15.9 and 21.8 ppm ^{1}H signals in the 2-^{13}C-acetone-loaded HPW and determine whether these H-bonding protons are much closer to the donor (i.e., HPW) or the acceptor (i.e., 2-^{13}C-acetone). Apparently, this important structural information cannot be obtained only through conventional ^{1}H NMR experiments.

Alternatively, the strength of the H-bonding interactions may also be featured through the electronic properties of the acceptors, as indicated by the ^{13}C NMR signals of adsorbed 2-^{13}C-acetone.[19,20] As shown in Figure 1B, the ^{13}C cross-

https://doi.org/10.1021/jacs.3c08723
J. Am. Chem. Soc. 2023, 145, 27471−27479

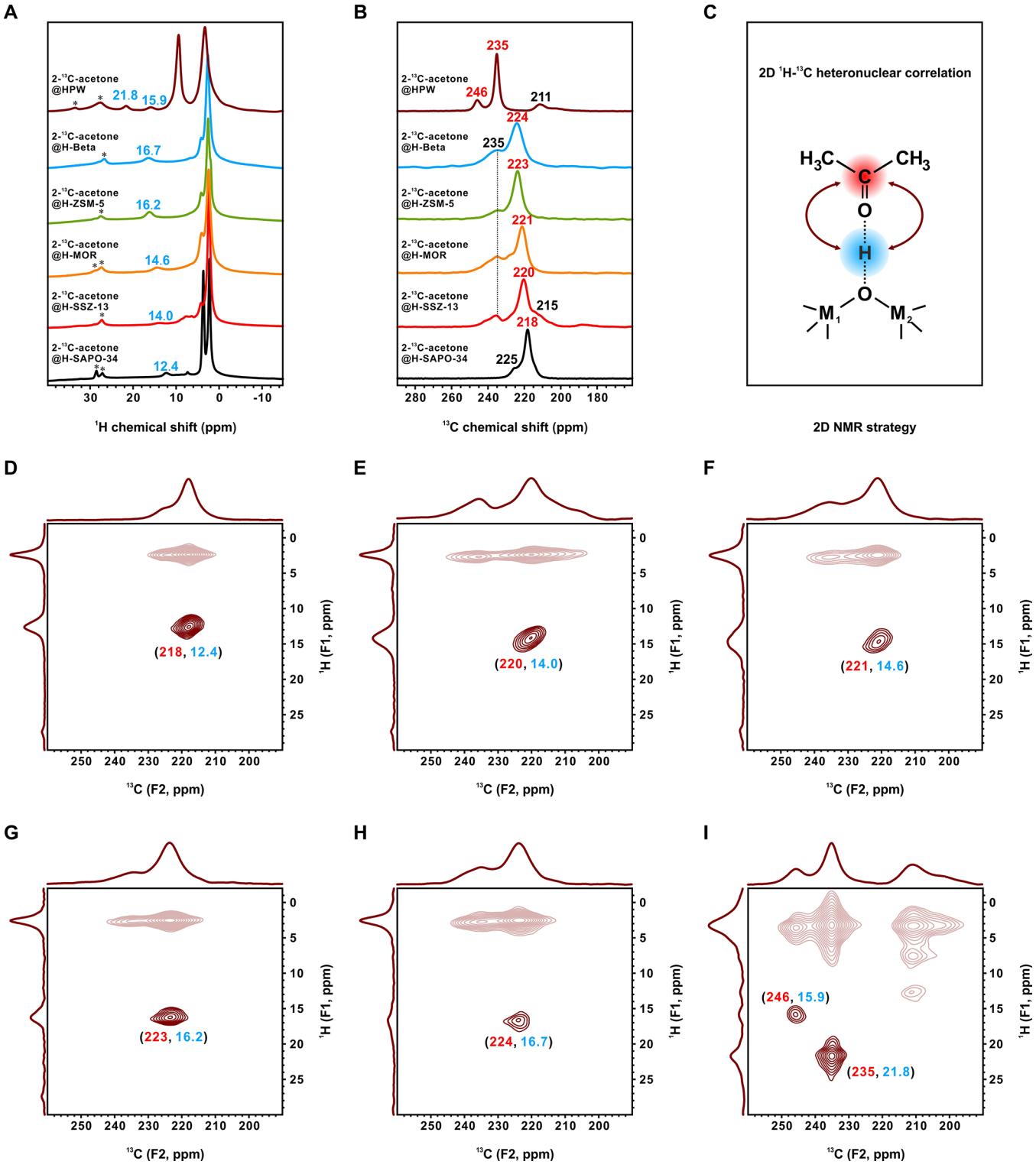

Figure 1. NMR results of various hydrogen-bonding interactions between acetone and distinct proton donors. 1D (A) ^{1}H MAS and (B) ^{13}C CP/MAS NMR spectra and 2D (C–I) ^{1}H–^{13}C heteronuclear correlation NMR spectra of various dehydrated acidic materials with 2-^{13}C-acetone adsorption: (D) H-SAPO-34, (E) H-SSZ-13, (F) H-MOR, (G) H-ZSM-5, (H) H-Beta, and (I) $H_3PW_{12}O_{40}$ (HPW). The Larmor frequencies for the ^{1}H and ^{13}C nucleus are 399.33 and 100.43 MHz, respectively. The MAS frequency is 12 kHz, and the CP contact time for the 2D heteronuclear correlation NMR experiments is 4 ms.

polarization (CP)/MAS NMR spectra of 2-^{13}C-acetone interacting with H-SAPO-34, H-SSZ-13, H-MOR, H-ZSM-5, and H-Beta zeolites revealed the main ^{13}C resonances at *ca.* 218, 220, 221, 223, and 224 ppm, respectively. Meanwhile, for the 2-^{13}C-acetone-loaded HPW, three characteristic peaks with δ^{13}C at 211, 235, and 246 ppm were observed. The resonances at 235 and 246 ppm can be assigned to 2-^{13}C-acetone bound to two different kinds of acidic protons with distinct proton-donating abilities, whereas the signal at 211 ppm likely arose from the products of the bimolecular and trimolecular

https://doi.org/10.1021/jacs.3c08723
J. Am. Chem. Soc. 2023, 145, 27471–27479

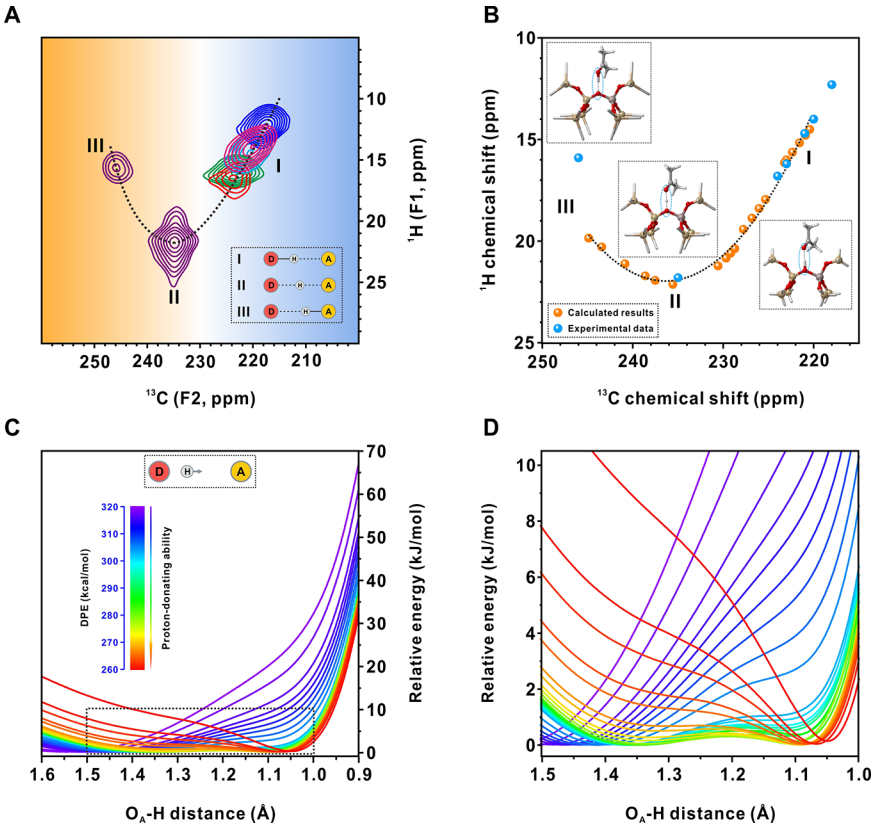

Figure 2. Correlations of proton donors and acceptors in various acetone hydrogen-bonding interactions. (A) Assorted 2D ^{1}H−^{13}C heteronuclear correlation NMR spectra of dehydrated H-SAPO-34, H-SSZ-13, H-MOR, H-ZSM-5, H-Beta, and HPW with 2-^{13}C-acetone adsorption. (B) Comparison between experimental and theoretically calculated ^{13}C and ^{1}H NMR chemical shifts of various H-bonding configurations with acetone adsorption. The ^{1}H and ^{13}C NMR chemical shifts were calculated using the gauge-independent atomic orbital method at the B3LYP/DZVP2 level. (C) Curves of the calculated relative energy and the relevant O$_A$−H distance between the H-bonding proton and the O atom of acetone in various H-bonding configurations via scanning the O$_A$−H spatial distance based on each optimized acetone adsorption geometry. (D) Enlarged view of the local region (marked with a black dotted line in C).

reactions (Aldol reaction) of 2-^{13}C-acetone,[34,35] similar to the 215 ppm ^{13}C resonance in H-SSZ-13. Furthermore, the minor ^{13}C signals at 225 ppm in H-SAPO-34 and at 235 ppm in H-SSZ-13, H-MOR, H-ZSM-5, and H-Beta may be originated from the coupling of 2-^{13}C-acetone with the Lewis acidic framework or extra-framework aluminum species[35] due to the dehydration treatment at an elevated temperature (673 K; Figure S1), *vide infra*. Thus, the proton-donating abilities of these typical proton donors were determined to be in the following order: HPW (δ^{13}C = 235, 246 ppm) > H-Beta (δ^{13}C = 224 ppm) > H-ZSM-5 (δ^{13}C = 223 ppm) > H-MOR (δ^{13}C = 221 ppm) > H-SSZ-13 (δ^{13}C = 220 ppm) > H-SAPO-34 (δ^{13}C = 218 ppm). However, the dependence of the ^{13}C signal of 2-^{13}C-acetone and the corresponding ^{1}H resonance of the H-bonding proton in a specific interaction configuration is still unclear. For example, it is unknown how to correlate the two ^{13}C signals (i.e., 235 and 246 ppm) and two ^{1}H resonances (i.e., 15.9 and 21.8 ppm) in the 2-^{13}C-acetone-loaded HPW. Apparently, the type and evolution of H-bonding interaction cannot be accurately identified through individual one-dimensional (1D) ^{1}H or ^{13}C NMR approaches using 2-^{13}C-acetone as a proton acceptor. A similar conclusion can also be obtained from the 1D NMR experiments with a basic TMPO acceptor (Figures S4 and S5).

Simultaneous Detection of the Chemical States of Proton Donors and Acceptors in Hydrogen-Bonding Interactions. Simultaneous observation of the electronic properties (i.e., NMR signals) of proton donors and acceptors is necessary, which would greatly facilitate the identification of the H-bonding types and the precise location of H atoms in various H-bonding configurations at the same time. Herein, a 2D ^{1}H−^{13}C heteronuclear correlation NMR technique[36] was employed to synchronously monitor the chemical shift variations of protons in the donors (^{1}H NMR signal) and carbonyl carbon atoms in the acceptors (^{13}C NMR signal) for various H-bonding interaction species (Figure 1C). This was achieved by simultaneously obtaining the isotropic chemical shift and spatial proximity information of ^{1}H and ^{13}C nuclei via ^{1}H→^{13}C CP relying on their through-space dipolar couplings[36] (Figure S6). We envisage that such a promising approach can provide invaluable information about the detailed local structures of various H-bonding configurations and thus overcome the unsolved issue of molecular visualization of H-bonding evolution.

As shown in Figure 1D, the correlation peaks at (225, 2.0) and (218, 2.0) ppm in the 2D ^{1}H−^{13}C heteronuclear correlation NMR spectrum of H-SAPO-34 with 2-^{13}C-acetone adsorption could be assigned to 2-^{13}C-acetone associated with the methyl protons. Furthermore, the correlation peak at (218, 12.4) ppm should originate from the H-bonding interaction complexes between adsorbed 2-^{13}C-acetone and H-bonding protons, which corresponded to the carbonyl carbon ^{13}C signal (F2 dimension) with a δ^{13}C of 218 ppm and the ^{1}H signal (F1

https://doi.org/10.1021/jacs.3c08723
J. Am. Chem. Soc. 2023, 145, 27471−27479

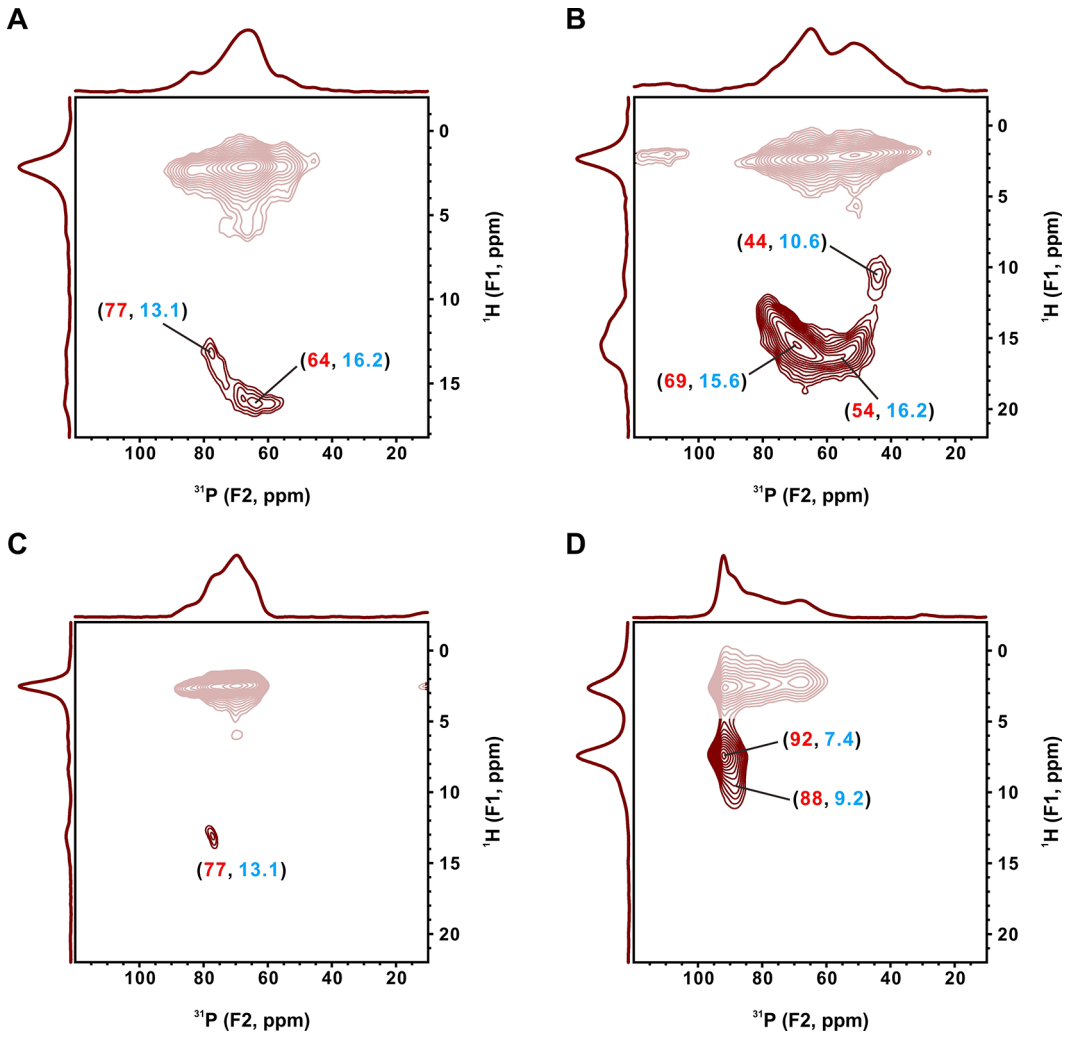

Figure 3. NMR results of various hydrogen-bonding interactions between TMPO and distinct proton donors. 2D ^{1}H−^{31}P heteronuclear correlation NMR spectra of various dehydrated acidic materials with TMPO adsorption: (A) H-MOR, (B) H-ZSM-5, (C) H-Beta, and (D) HPW. The Larmor frequencies for the ^{1}H and ^{31}P nucleus are 399.33 and 161.90 MHz, respectively. The MAS frequency is 12 kHz, and the CP contact time for the 2D heteronuclear correlation NMR experiments is 4 ms.

dimension) with a δ^{1}H of 12.4 ppm. Note that no correlation peak was observed between the ^{13}C signal at 225 ppm and the proton in the H-bonding complexes. This was because the 225 ppm ^{13}C resonance originated from the 2-^{13}C-acetone directly adsorbed on the Lewis acidic framework or extra-framework aluminum species.[35] Other H-bonding complexes could also be identified in 2-^{13}C-acetone-loaded H-SSZ-13, H-MOR, H-ZSM-5, and H-Beta zeolites, as evidenced by the appearance of correlation peak signals at (220, 14.0), (221, 14.6), (223, 16.2), and (224, 16.7) ppm, respectively, in their corresponding 2D ^{1}H−^{13}C heteronuclear correlation NMR spectra (Figure 1E−H). Furthermore, two different kinds of H-bonding interaction complexes were observed when 2-^{13}C-acetone interacted with strongly acidic HPW, which corresponded to correlation peaks at (235, 21.8) and (246, 15.9) ppm (Figure 1I).

In particular, based on the 2D ^{1}H−^{13}C correlation NMR experimental results, it is fascinating to note that a parabola-shaped contour can be derived. As shown in Figure 2A, the δ^{13}C of the carbonyl group in the adsorbed 2-^{13}C-acetone gradually increased upon increasing the proton-donating ability of the various acidic materials (i.e., 218 ppm for H-SAPO-34, 220 ppm for H-SSZ-13, 221 ppm for H-MOR, 223 ppm for H-ZSM-5, 224 ppm for H-Beta, and 235 and 246 ppm for HPW). However, the corresponding δ^{1}H of the H-bonding proton first increased from 12.4 ppm in H-SAPO-34 to 14.0 ppm in H-SSZ-13, 14.6 ppm in H-MOR, 16.2 ppm in H-ZSM-5, 16.7 ppm in H-Beta, and 21.8 ppm in HPW, and then, it dramatically decreased to 15.9 ppm in HPW. Undoubtedly, compared to conventional 1D ^{1}H and ^{13}C NMR, the 2D ^{1}H−^{13}C heteronuclear correlation technique manifested its unique advantage for simultaneously monitoring the electronic properties of protons in the donors and carbonyl carbon atoms in the acceptors through their chemical shifts. Thus, more detailed structural information on various H-bonding configurations with subtle distinctions may be obtained.

Owing to the weaker proton-donating ability, H-SAPO-34, H-SSZ-13, H-MOR, H-ZSM-5, and H-Beta zeolites are conventionally impotent in protonating weakly basic acetone. Therefore, the corresponding acetone adsorption configurations in these acidic materials can be classified as weak H-bonding interactions in which the protons are still linked to donors (Scheme 1A). Nevertheless, due to the stronger proton-donating ability of HPW, a strong H-bonding

https://doi.org/10.1021/jacs.3c08723
J. Am. Chem. Soc. 2023, 145, 27471−27479

configuration was formed with the 2D $^{1}H-^{13}C$ correlation signal at (235, 21.8) ppm, where the proton was almost located right in the middle between HPW (i.e., proton donor) and acetone (i.e., proton acceptor) (Scheme 1C). Note that this kind of ultrastrong H-bonding interaction resulted in a significant deshielding effect of the hydrogen nuclei, leading to a highly ionized proton with an unprecedented large ^{1}H chemical shift at 21.8 ppm. Meanwhile, HPW also possesses another kind of acidic proton with a superstrong proton-donating ability, enabling it to protonate weakly basic acetone ($\delta^{13}C$ = 246 ppm), resulting in an ion-pair adsorption configuration, which indicated a weak H-bonding interaction as well (Scheme 1E). It is noted that the proton was now transferred to link with acetone. As a consequence, the detailed types and relevant evolution of various H-bonding configurations during the acetone protonation process have been clearly identified by using advanced 2D heteronuclear correlation NMR experiments, which are far superior to conventional characterization techniques and 1D NMR methods.

To verify the universality of 2D NMR approaches in identifying the H-bonding types during proton transfer, 2D $^{1}H-^{31}P$ heteronuclear correlation NMR experiments in combination with a TMPO acceptor were also performed, as shown in Figures 3 and 4. Herein, it should be noted that due

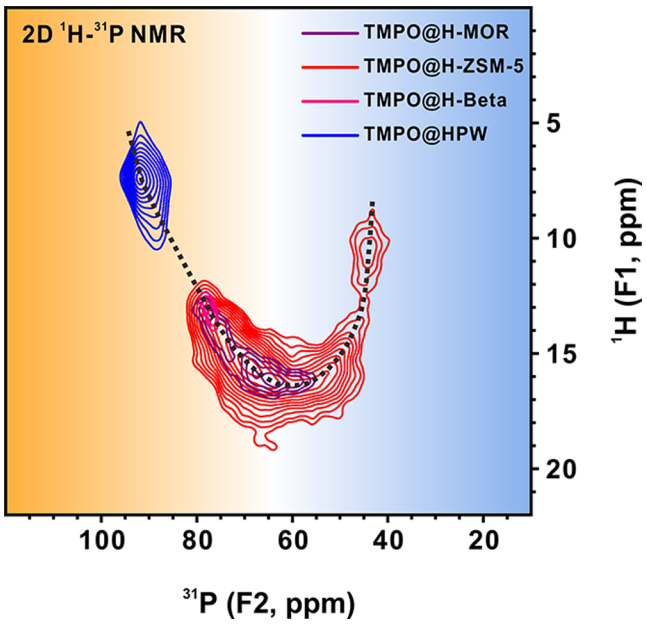

Figure 4. Assorted 2D $^{1}H-^{31}P$ heteronuclear correlation NMR spectra of dehydrated H-MOR, H-ZSM-5, H-Beta, and HPW with TMPO adsorption.

to the stronger basicity and larger molecular size of TMPO compared to 2-^{13}C-acetone, it is generally difficult for the adsorbed TMPO complexes to do fast exchange among different adsorption sites inside zeolites (e.g., H-ZSM-5); thus, the distribution of Brønsted acidic protons with different proton-donating abilities can be detected, rendering more complicated H-bonding interaction signals. Nevertheless, a similar parabola-shaped correlation was obtained as well, demonstrating again that the 2D heteronuclear correlation NMR techniques are powerful and sensitive in identifying the detailed local fine structures with subtle distinctions in various molecular configurations.

Dynamic Evolution Processes of Hydrogen-Bonding Interactions. Quantum chemical calculations were further conducted to render more fundamental insights into the diverse H-bonding interactions and their evolution at the atomic level. Figure 2B illustrates the relationship between the calculated ^{13}C and ^{1}H chemical shifts of various acetone adsorption configurations with subtle distinctions over a series of donors with different proton-donating abilities (Figures S7 and S8), which revealed excellent agreement with our 2D NMR experimental data and further elucidated the availability, sensitivity, and potentiality of advanced 2D heteronuclear correlation NMR approaches for precise structural identification. Furthermore, by theoretically scanning the O_A-H spatial distance between the H-bonding proton and the O atom of acetone, we also plotted the curves of their calculated relative energies based on each optimized H-bonding configuration. As shown in Figure 2C and enlarged in Figure 2D, the potential energy surface (PES) of the acetone adsorption complexes over donors with weaker proton-donating abilities only gave rise to a single-well PES. With an increase in the proton-donating ability of the donor, a double-well PES gradually emerged. In particular, an approximately flat-bottom double-well PES with a nearly negligible energy barrier was observed when the proton-donating ability of the donor exactly increased to a certain extent, corresponding to a strong H-bonding interaction, in which the H-bonding proton was precisely centered and equally shared between the donor and acceptor. Upon further increasing the proton-donating ability, the H-bonding proton tended to protonate acetone, and eventually, a single-well PES reappeared.

In general, the single-well PES suggests that there is only one energy minimum point, indicating that the H-bonding proton is exclusively bonded to the donor or the acceptor and that the proton transfer is almost irreversible. In contrast, the double-well PES suggests that there are two energy minimum points, indicating that the proton transfer from the donor to the acceptor or from the acceptor to the donor is comparable and reversible. Herein, note that the electronegativity of the O atom in the proton donor was precisely manipulated through theoretically adjusting the acidic models (Figures S7 and S8). Meanwhile, the electronegativity of the O atom in the proton acceptor (i.e., acetone) remains actually unchanged. Then, when the electronegativity difference between the O atom in the proton donor and acceptor is large enough, the PES for proton transfer will be an insurmountable single well. Otherwise, when the electronegativity of the O atom in the proton donor is comparable to that in the acceptor, a competitive attractive interaction with the H-bonding proton will occur, as anticipated, rendering a double-well PES for proton transfer. Obviously, these theoretical results were in good agreement with our experimental conjecture in Scheme 1.

To monitor the H-bonding evolution from the perspective of the electronic level, we further theoretically traced the acetone protonation process over a given proton donor with a deprotonation energy (DPE) of 280 kcal/mol. Accordingly, five specific states (i.e., I' and local minimum I: the proton is linked to the donor; II: transition state configuration; III' and local minimum III: the proton is linked to the acceptor; Figure 5A) on the potential energy surface were selected to analyze their electronic properties based on the electron localization

https://doi.org/10.1021/jacs.3c08723
J. Am. Chem. Soc. 2023, 145, 27471−27479

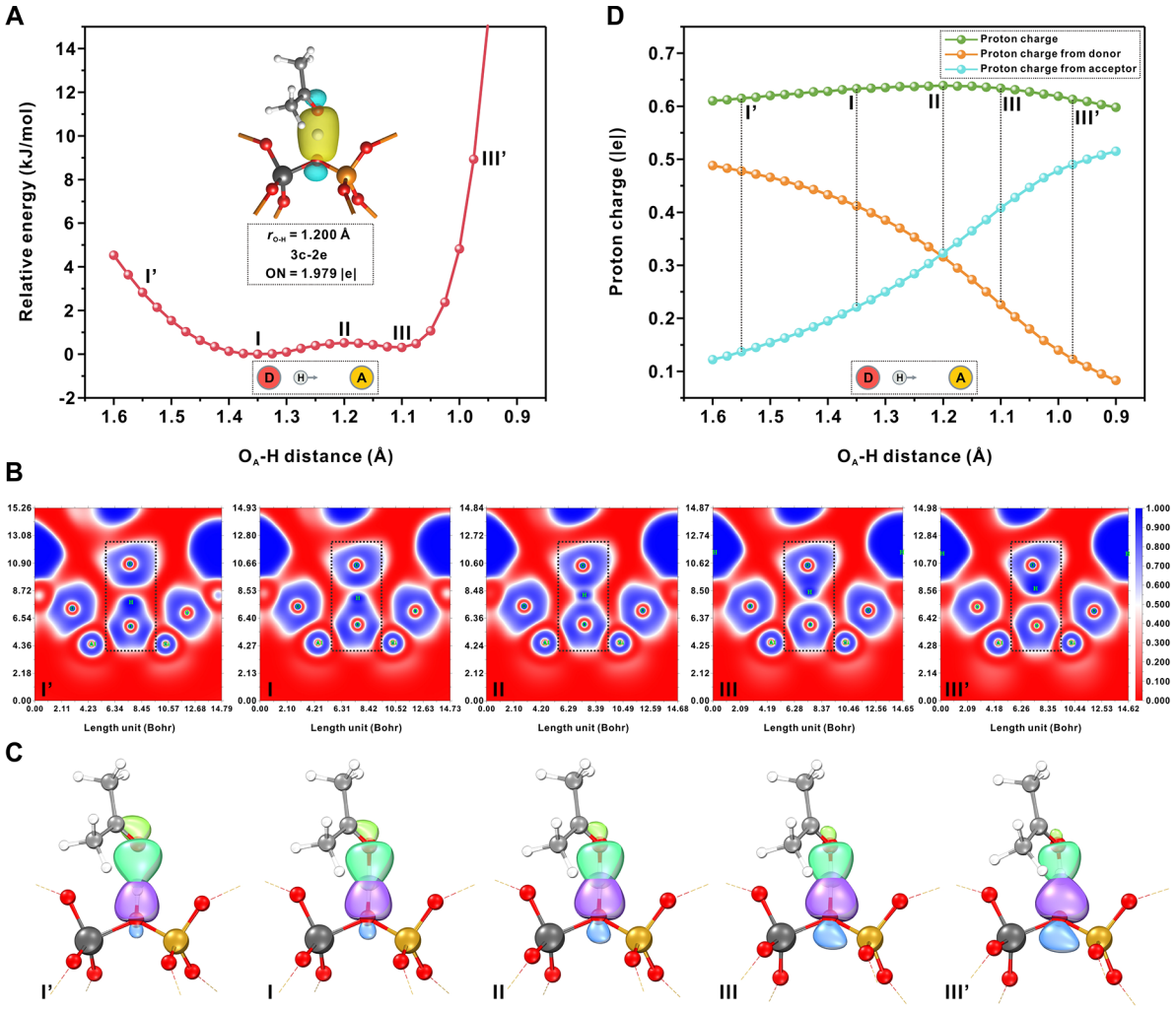

Figure 5. Theoretical results of the dynamic evolution of hydrogen-bonding interactions during the acetone protonation process. (A) Potential energy surface of proton transfer from a given proton donor with the DPE of 280 kcal/mol to acetone; the inset image is the AdNDP analysis result of state II (ON: occupation number). (B) ELF and (C) IBO graphs of states I', I, II, III, and III' in A. Purple and blue balls: the σ orbital of the O_D−H bond in the proton donor → the p lone pair of the O atom; green and yellow balls: the p lone pair of the O atom → the σ orbital of the O_A−H bond in the acceptor. (D) Total charge of the H-bonding proton and that respectively originating from the donor and acceptor along the proton transfer process.

function (ELF),[37,38] intrinsic bond orbital (IBO),[39,40] relevant atomic charge, and adaptive natural density partitioning (AdNDP) methods.[41] Thereinto, 2D ELF analysis was used to identify the covalent characteristics of the chemical bonds in various H-bonding configurations. A larger ELF value normally indicates a more covalent chemical bond.[37,38] The 2D ELF images in Figure 5B clearly revealed the gradual transformation of the covalent O_D−H bond between the H-bonding proton and donor (I' and I) to the transition state (II) and then to the covalent O_A−H bond between the H-bonding proton and acceptor (III and III'). The proton transfer process can also be interpreted as the variation of two IBOs (i.e., the σ orbital of the O_D−H bond in the proton donor and the σ orbital of the O_A−H bond in the acceptor). Figure 5C illustrates the synchronous evolution of these two IBOs during the acetone protonation process, that is, the σ orbital of the O_D−H bond in the proton donor → the p lone pair of the O atom and the p lone pair of the O atom → the σ orbital of the O_A−H bond in the acceptor. Thus, the evolution of the H-bonding interactions has been accurately identified and visualized at the electronic level.

Moreover, it is well-accepted that the hydrogen atomic charge is closely associated with its detailed electronic characteristics, which is therefore of great relevance to the involved NMR shielding of the ^{1}H nucleus. Generally, a larger hydrogen atomic charge corresponds to a larger ^{1}H NMR chemical shift.[42,43] Herein, it was found that the atomic charge of the H-bonding proton (Q_H^+) contributed from the O_D atom in the donor gradually decreased with the shortening of the O_A−H spatial distance, in contrast to that from the O_A atom in acetone. In particular, the total Q_H^+ increased to the maximum exactly at transition state II; then, it began to decrease when the proton was closer to acetone (Figure 5D). This may be caused by the typical electron delocalization characteristic of transition state II, as indicated by the remarkable three-center two-electron (3c-2e) orbital with an occupation number of 1.979 |e| through AdNDP analysis (Figure 5A). Thus, the hydrogen atomic charge variation during the acetone protonation process also functioned as a parabola-shaped correlation, which is in excellent agreement with our NMR experimental results (Figure 2A). Undoubtedly, compared to conventional analytical methods to characterize the electronic

https://doi.org/10.1021/jacs.3c08723
J. Am. Chem. Soc. 2023, 145, 27471−27479

properties (e.g., X-ray photoelectron spectroscopy),[44,45] the 2D heteronuclear correlation NMR technique manifests its advantage on simultaneously monitoring the variations of the NMR shielding for the proton donor and the acceptor, which are closely related to the corresponding atomic charge as well, thus enabling them to largely facilitate the direct molecular description of the types and evolution processes of various H-bonding interactions.

CONCLUSIONS

In summary, our work sheds light on the precise molecular description of the types and dynamic evolution of various H-bonding interactions during proton transfer processes. For the first time, a highly ionized hydrogen with an unprecedented large ^{1}H chemical shift at 21.8 ppm due to the high electron delocalization of ultrastrong H-bonding interactions has been clearly revealed by using a combined NMR experiment and quantum calculation approach. These results should provide new insights toward our fundamental understanding of the origins, definitions, and types of H-bonding interactions and confirm the superiority of advanced 2D heteronuclear correlation NMR techniques in identifying the subtle distinctions of local fine structures in various molecular configurations in the H-bonding systems.

ASSOCIATED CONTENT

Supporting Information

The Supporting Information is available free of charge at https://pubs.acs.org/doi/10.1021/jacs.3c08723.

Detailed experimental and theoretical calculation methods, as well as additional ^{27}Al, ^{29}Si, and ^{1}H MAS NMR spectra of various acidic materials, and the 1D ^{1}H and ^{31}P CP/MAS NMR experimental results for various acidic materials with the adsorption of the TMPO molecule, including Figures S1−S8 (PDF)

AUTHOR INFORMATION

Corresponding Author

Anmin Zheng − *Interdisciplinary Institute of NMR and Molecular Sciences, School of Chemistry and Chemical Engineering, The State Key Laboratory of Refractories and Metallurgy, Wuhan University of Science and Technology, Wuhan 430081, P. R. China; State Key Laboratory of Magnetic Resonance and Atomic and Molecular Physics, National Center for Magnetic Resonance in Wuhan, Wuhan Institute of Physics and Mathematics, Innovation Academy for Precision Measurement Science and Technology, Chinese Academy of Sciences, Wuhan 430071, P. R. China;* orcid.org/0000-0001-7115-6510; Email: zhenganm@wipm.ac.cn

Authors

Xianfeng Yi − *State Key Laboratory of Magnetic Resonance and Atomic and Molecular Physics, National Center for Magnetic Resonance in Wuhan, Wuhan Institute of Physics and Mathematics, Innovation Academy for Precision Measurement Science and Technology, Chinese Academy of Sciences, Wuhan 430071, P. R. China;* orcid.org/0000-0001-9224-3111

Wei Chen − *State Key Laboratory of Magnetic Resonance and Atomic and Molecular Physics, National Center for Magnetic Resonance in Wuhan, Wuhan Institute of Physics and Mathematics, Innovation Academy for Precision Measurement Science and Technology, Chinese Academy of Sciences, Wuhan 430071, P. R. China;* orcid.org/0000-0002-8955-9497

Yao Xiao − *State Key Laboratory of Magnetic Resonance and Atomic and Molecular Physics, National Center for Magnetic Resonance in Wuhan, Wuhan Institute of Physics and Mathematics, Innovation Academy for Precision Measurement Science and Technology, Chinese Academy of Sciences, Wuhan 430071, P. R. China*

Fengqing Liu − *State Key Laboratory of Magnetic Resonance and Atomic and Molecular Physics, National Center for Magnetic Resonance in Wuhan, Wuhan Institute of Physics and Mathematics, Innovation Academy for Precision Measurement Science and Technology, Chinese Academy of Sciences, Wuhan 430071, P. R. China; University of Chinese Academy of Sciences, Beijing 100049, P. R. China*

Xin Yu − *State Key Laboratory of Magnetic Resonance and Atomic and Molecular Physics, National Center for Magnetic Resonance in Wuhan, Wuhan Institute of Physics and Mathematics, Innovation Academy for Precision Measurement Science and Technology, Chinese Academy of Sciences, Wuhan 430071, P. R. China; University of Chinese Academy of Sciences, Beijing 100049, P. R. China*

Complete contact information is available at: https://pubs.acs.org/10.1021/jacs.3c08723

Notes

The authors declare no competing financial interest.

ACKNOWLEDGMENTS

This work was supported by the National Natural Science Foundation of China (nos. 22125304, 22032005, 22002174, 22241801, 21991090, and 21991092) and the National Key R&D Program of China (nos. 2021YFA1502600 and 2022YFE0116000).

REFERENCES

(1) Yang, J.; Dettori, R.; Nunes, J. P. F.; List, N. H.; Biasin, E.; Centurion, M.; Chen, Z.; Cordones, A. A.; Deponte, D. P.; Heinz, T. F.; et al. Direct observation of ultrafast hydrogen bond strengthening in liquid water. *Nature* **2021**, *596*, 531−535.

(2) Smith, J. D.; Cappa, C. D.; Wilson, K. R.; Cohen, R. C.; Geissler, P. L.; Saykally, R. J. Unified description of temperature-dependent hydrogen-bond rearrangements in liquid water. *Proc. Natl. Acad. Sci. USA* **2005**, *102*, 14171−14174.

(3) Dong, J.; Davis, A. P. Molecular recognition mediated by hydrogen bonding in aqueous media. *Angew. Chem., Int. Ed.* **2021**, *60*, 8035−8048.

(4) Jena, S.; Dutta, J.; Tulsiyan, K. D.; Sahu, A. K.; Choudhury, S. S.; Biswal, H. S. Noncovalent interactions in proteins and nucleic acids: Beyond hydrogen bonding and π-stacking. *Chem. Soc. Rev.* **2022**, *51*, 4261−4286.

(5) Zhang, J.; Chen, P.; Yuan, B.; Ji, W.; Cheng, Z.; Qiu, X. Real-space identification of intermolecular bonding with atomic force microscopy. *Science* **2013**, *342*, 611−614.

(6) Pfriem, N.; Hintermeier, P. H.; Eckstein, S.; Kim, S.; Liu, Q.; Shi, H.; Milakovic, L.; Liu, Y.; Haller, G. L.; Baráth, E.; Liu, Y.; Lercher, J. A. Role of the ionic environment in enhancing the activity of reacting molecules in zeolite pores. *Science* **2021**, *372*, 952−957.

(7) Fu, J.; Liu, S.; Zheng, W.; Huang, R.; Wang, C.; Lawal, A.; Alexopoulos, K.; Liu, S.; Wang, Y.; Yu, K.; et al. Modulating the dynamics of Brønsted acid sites on $PtWO_x$ inverse catalyst. *Nat. Catal.* **2022**, *5*, 144−153.

(8) Martínez-Espín, J. S.; De Wispelaere, K.; Janssens, T. V.; Svelle, S.; Lillerud, K. P.; Beato, P.; Van Speybroeck, V.; Olsbye, U. Hydrogen transfer versus methylation: On the genesis of aromatics formation in the methanol-to-hydrocarbons reaction over H-ZSM-5. *ACS Catal.* **2017**, *7*, 5773−5780.
(9) Chizallet, C.; Bouchy, C.; Larmier, K.; Pirngruber, G. Molecular views on mechanisms of Brønsted acid-catalyzed reactions in zeolites. *Chem. Rev.* **2023**, *123*, 6107−6196.
(10) Arunan, E.; Desiraju, G. R.; Klein, R. A.; Sadlej, J.; Scheiner, S.; Alkorta, I.; Clary, D. C.; Crabtree, R. H.; Dannenberg, J. J.; Hobza, P.; et al. Definition of the hydrogen bond (IUPAC Recommendations 2011). *Pure Appl. Chem.* **2011**, *83*, 1637−1641.
(11) Grabowski, S. J. *Understanding hydrogen bonds: Theoretical and experimental views*. Royal Society of Chemistry, 2020.
(12) Khudozhitkov, A. E.; Stange, P.; Golub, B.; Paschek, D.; Stepanov, A. G.; Kolokolov, D. I.; Ludwig, R. Characterization of doubly ionic hydrogen bonds in protic ionic liquids by NMR deuteron quadrupole coupling constants: Differences to H-bonds in amides, peptides, and proteins. *Angew. Chem., Int. Ed.* **2017**, *56*, 14310−14314.
(13) Lobato, A.; Salvadó, M. A.; Recio, J. M.; Taravillo, M.; Baonza, V. G. Highs and lows of bond lengths: Is there any limit? *Angew. Chem., Int. Ed.* **2021**, *60*, 17028−17036.
(14) Civiš, S.; Lamanec, M.; Špirko, V.; Kubišta, J.; Špeťko, M.; Hobza, P. Hydrogen bonding with hydridic hydrogen-experimental low-temperature IR and computational study: Is a revised definition of hydrogen bonding appropriate? *J. Am. Chem. Soc.* **2023**, *145*, 8550−8559.
(15) Dereka, B.; Yu, Q.; Lewis, N. H.; Carpenter, W. B.; Bowman, J. M.; Tokmakoff, A. Crossover from hydrogen to chemical bonding. *Science* **2021**, *371*, 160−164.
(16) Bonn, M.; Hunger, J. Between a hydrogen and a covalent bond. *Science* **2021**, *371*, 123−124.
(17) Yin, Z.; Chang, Y. P.; Balčiūnas, T.; Shakya, Y.; Djorović, A.; Gaulier, G.; Fazio, G.; Santra, R.; Inhester, L.; Wolf, J. P.; Wörner, H. J. Femtosecond proton transfer in urea solutions probed by X-ray spectroscopy. *Nature* **2023**, *619*, 749−754.
(18) Corma, A. Inorganic solid acids and their use in acid-catalyzed hydrocarbon reactions. *Chem. Rev.* **1995**, *95*, 559−614.
(19) Haw, J. F.; Xu, T.; Nicholas, J. B.; Goguen, P. W. Solvent-assisted proton transfer in catalysis by zeolite solid acids. *Nature* **1997**, *389*, 832−835.
(20) Barich, D. H.; Nicholas, J. B.; Xu, T.; Haw, J. F. Theoretical and experimental study of the ^{13}C chemical shift tensors of acetone complexed with Brønsted and Lewis acids. *J. Am. Chem. Soc.* **1998**, *120*, 12342−12350.
(21) Yi, X.; Ko, H.; Deng, F.; Liu, S.; Zheng, A. Solid-state ^{31}P NMR mapping of active centers and relevant spatial correlations in solid acid catalysts. *Nat. Protoc.* **2020**, *15*, 3527−3555.
(22) Peng, Y.-K.; Tsang, S. C. E. Probe-assisted NMR: Recent progress on the surface study of crystalline metal oxides with various terminated facets. *Magn. Reson. Lett.* **2022**, *2*, 9−16.
(23) Bornes, C.; Fischer, M.; Amelse, J. A.; Geraldes, C. F.; Rocha, J.; Mafra, L. What is being measured with P-bearing NMR probe molecules adsorbed on zeolites? *J. Am. Chem. Soc.* **2021**, *143*, 13616−13623.
(24) Klinowski, J. Solid-state NMR studies of molecular sieve catalysts. *Chem. Rev.* **1991**, *91*, 1459−1479.
(25) Jiang, Y.; Huang, J.; Dai, W.; Hunger, M. Solid-state nuclear magnetic resonance investigations of the nature, property, and activity of acid sites on solid catalysts. *Solid State Nucl. Magn. Reson.* **2011**, *39*, 116−141.
(26) Chen, K.; Abdolrhamani, M.; Sheets, E.; Freeman, J.; Ward, G.; White, J. L. Direct detection of multiple acidic proton sites in zeolite HZSM-5. *J. Am. Chem. Soc.* **2017**, *139*, 18698−18704.
(27) Yates, J. R.; Pham, T. N.; Pickard, C. J.; Mauri, F.; Amado, A. M.; Gil, A. M.; Brown, S. P. An investigation of weak CH···O hydrogen bonds in maltose anomers by a combination of calculation and experimental solid-state NMR spectroscopy. *J. Am. Chem. Soc.* **2005**, *127*, 10216−10220.
(28) Uldry, A. C.; Griffin, J. M.; Yates, J. R.; Pérez-Torralba, M.; Santa María, M. D.; Webber, A. L.; Beaumont, M. L. L.; Samoson, A.; Claramunt, R. M.; Pickard, C. J.; Brown, S. P. Quantifying weak hydrogen bonding in uracil and 4-cyano-4'-ethynylbiphenyl: a combined computational and experimental investigation of NMR chemical shifts in the solid state. *J. Am. Chem. Soc.* **2008**, *130*, 945−954.
(29) Štoček, J. R.; Socha, O.; Císařová, I.; Slanina, T.; Dračínský, M. Importance of nuclear quantum effects for molecular cocrystals with short hydrogen bonds. *J. Am. Chem. Soc.* **2022**, *144*, 7111−7116.
(30) Schroeder, C.; Zones, S. I.; Hansen, M. R.; Koller, H. Hydrogen bonds dominate Brønsted acid sites in zeolite SSZ-42: A classification of their diversity. *Angew. Chem., Int. Ed.* **2022**, *61*, No. e202109313.
(31) Kong, X.; Deng, H.; Yan, F.; Kim, J.; Swisher, J. A.; Smit, B.; Yaghi, O. M.; Reimer, J. A. Mapping of functional groups in metal-organic frameworks. *Science* **2013**, *341*, 882−885.
(32) Yarulina, I.; De Wispelaere, K.; Bailleul, S.; Goetze, J.; Radersma, M.; Abou-Hamad, E.; Vollmer, I.; Goesten, M.; Mezari, B.; Hensen, E. J. M.; et al. Structure-performance descriptors and the role of Lewis acidity in the methanol-to-propylene process. *Nat. Chem.* **2018**, *10*, 804−812.
(33) Trickett, C. A.; Osborn Popp, T. M.; Su, J.; Yan, C.; Weisberg, J.; Huq, A.; Urban, P.; Jiang, J.; Kalmutzki, M. J.; Liu, Q.; et al. Identification of the strong Brønsted acid site in a metal-organic framework solid acid catalyst. *Nat. Chem.* **2019**, *11*, 170−176.
(34) Yang, J.; Janik, M. J.; Ma, D.; Zheng, A.; Zhang, M.; Neurock, M.; Davis, R. J.; Ye, C.; Deng, F. Location, acid strength, and mobility of the acidic protons in Keggin 12-$H_3PW_{12}O_{40}$: A combined solid-state NMR spectroscopy and DFT quantum chemical calculation study. *J. Am. Chem. Soc.* **2005**, *127*, 18274−18280.
(35) Biaglow, A. I.; Gorte, R. J.; White, D. ^{13}C NMR studies of acetone in dealuminated faujasites: A probe for nonframework alumina. *J. Catal.* **1994**, *150*, 221−224.
(36) Brown, S. P.; Spiess, H. W. Advanced solid-state NMR methods for the elucidation of structure and dynamics of molecular, macromolecular, and supramolecular systems. *Chem. Rev.* **2001**, *101*, 4125−4156.
(37) Silvi, B.; Savin, A. Classification of chemical bonds based on topological analysis of electron localization functions. *Nature* **1994**, *371*, 683−686.
(38) Petit, L.; Joubert, L.; Maldivi, P.; Adamo, C. A comprehensive theoretical view of the bonding in actinide molecular complexes. *J. Am. Chem. Soc.* **2006**, *128*, 2190−2191.
(39) Glendening, E. D.; Landis, C. R.; Weinhold, F. Natural bond orbital methods. *WIREs Comput. Mol. Sci.* **2012**, *2*, 1−42.
(40) Knizia, G. Intrinsic atomic orbitals: An unbiased bridge between quantum theory and chemical concepts. *J. Chem. Theory Comput.* **2013**, *9*, 4834−4843.
(41) Zubarev, D. Y.; Boldyrev, A. I. Developing paradigms of chemical bonding: adaptive natural density partitioning. *Phys. Chem. Chem. Phys.* **2008**, *10*, 5207−5217.
(42) Gun'ko, V. M.; Turov, V. V. Structure of hydrogen bonds and ^1H NMR spectra of water at the interface of oxides. *Langmuir* **1999**, *15*, 6405−6415.
(43) Zheng, A.; Zhang, H.; Chen, L.; Yue, Y.; Ye, C.; Deng, F. Relationship between ^1H chemical shifts of deuterated pyridinium ions and Brønsted acid strength of solid acids. *J. Phys. Chem. B* **2007**, *111*, 3085−3089.
(44) Greczynski, G.; Haasch, R. T.; Hellgren, N.; Lewin, E.; Hultman, L. X-ray photoelectron spectroscopy of thin films. *Nat. Rev. Methods Primers* **2023**, *3*, 40.
(45) Wang, H.; Soldemo, M.; Degerman, D.; Lömker, P.; Schlueter, C.; Nilsson, A.; Amann, P. Direct evidence of subsurface oxygen formation in oxide-derived Cu by X-ray photoelectron spectroscopy. *Angew. Chem., Int. Ed.* **2022**, *61*, No. e202111021.

https://doi.org/10.1021/jacs.3c08723
J. Am. Chem. Soc. 2023, 145, 27471−27479